Progress In Electromagnetics Research C, Vol. 98, 17–30, 2020

Direct Suspension Control Based on Second Order Sliding Mode for Bearingless Brushless DC Motor

Baohua Yue[1], Ye Yuan[2, *], and Tianyue Tao[2]

Abstract—For direct suspension force control (DSFC) strategy of Bearingless Brushless DC Motor (BBLDCM), combined with super-twisting algorithm, a second-order sliding mode (SOSM) controler is designed by direct suspension force. The control precision, robustness, and jitter suppression of the suspension subsystem are improved. The direct suspension force control based on the second-order sliding mode (SOSM-DSFC) solves the influence of external disturbance on the self-stabilizing suspension, effectively suppresses the rotor jitter problem, and improves the robustness of the rotor suspension.

1. INTRODUCTION

BBLDCM is based on the traditional permanent magnet brushless DC motor, adding a set of suspension windings to break the air gap magnetic field to generate suspension force [1]. It also has the advantages of bearingless motor of high integration, no mechanical wear, long service life, and no pollution [2]. BBLDCM has high research value and wide application prospects in biomedical fields such as blood pumps, high-speed/ultra-high-speed centrifuges, surgical cutting chainsaws, new energy fields, e.g., flywheel energy storage and aerospace [3–9].

BBLDCM is a strong coupling and nonlinear system [10]. Therefore, it is difficult to accurately control the radial suspension force of the rotor and rotor shakes seriously [11]. Ref. [12] adopts a three-phase simultaneous conduction control of the suspension force winding which achieves a stable suspension of the rotor; however, the power consumption is great. Refs. [13, 14] propose a current hysteretic suspension force control method. This method is limited by the width of hysteresis loop and the operating frequency of switching device, and the switching loss is large. Due to the linear relationship between the inductance of the suspension winding and the rotor displacement, a self-detection method for estimating the radial displacement of the rotor based on the high-frequency signal injection of the suspension winding is proposed in [15]. This method saves the cost of the eddy current displacement sensor but reduces operational reliability. Ref. [16] proposes a DSFC algorithm based on space vector pulse width modulation. SVPWM method is used to adjust the change of the suspension winding flux linkage to realize the closed-loop control of the suspension force and weaken the rotor jitter. The algorithm requires cumbersome coordinate transformations and complex calculations. When system parameters change or are affected by external uncertainties, the PID control no longer meets the requirements of high performance. Sliding mode control has the characteristics of fast response, insensitivity to disturbance and parameter change, and simple implementation. It is widely used in motor control. However, the first-order sliding mode control has discontinuous and severe chattering problems, which affect the control effect of the system. In this frame, high-order sliding mode control acts on the high-order derivative with discontinuous control input and retains the advantages of traditional

Received 16 September 2019, Accepted 26 November 2019, Scheduled 19 December 2019
* Corresponding author: Ye Yuan (763874393@qq.com).
[1] College of Information Engineering, Xinyang Agriculture and Forestry University, Xinyang 464000, China. [2] School of Electrical and Information Engineering, Jiangsu University, Zhenjiang 212013, China.

sliding mode. The idea of high-order sliding mode control is proposed in [17]. Ref. [18] applies high-order sliding mode control for the nonlinear control of an induction motor, which improves the static and dynamic performance of motor speed regulation and enhances the robustness.

In order to improve the control precision of the radial suspension force of the BBLDCM, a DSFC strategy is proposed in [19], which is based on the traditional brushless DC direct torque [20, 21] control and different from direct suspension force control of space vector pulse width modulation. Inspired by [19], this paper introduces the SOSM of super twisting algorithm based on the DSFC and designs the direct suspension force control based on SOSM. Firstly, the basic principle of DSFC is introduced, and then a sliding mode displacement controller is designed. Taking the x-axis single-degree-of-freedom displacement of the rotor as an example, the radial suspension force F_x in the x-axis direction of the rotor is defined as control quantity u. Super twisting algorithm is adopted, and the second-order sliding mode is improved to realize the second-order sliding mode direct suspension force control. The control results show that the second-order sliding mode direct suspension force control is feasible and effective.

2. BBLDCM DIRECT SUSPENSION FORCE CONTROL

2.1. The Mechanism of Suspension Force Generation

BBLDCM embeds a set of suspension control windings in stator slots of the brushless DC motor, so that the suspension magnetic field and rotating magnetic field share a set of core magnetic circuit.

Figure 1 is a schematic diagram of an external rotor BBLDCM. $a1$, $a2$, $b1$, $b2$, $c1$, and $c2$ are suspension windings of the motor. Each set of windings is composed of two windings in series. When $a1$ winding passes into the current in the direction shown in the figure, the magnetic force at air gap 1 decreases. Conversely, the magnetic density at air gap 2 increases, thereby breaking the balance of the air gap magnetic density on both sides of the rotor and generating the suspension force that displaces the rotor along axis $+x$. Similarly, when suspension winding $a2$ is supplied with current as shown, a suspension force is generated which causes the rotor to move along axis $+y$. Therefore, by changing the magnitude and direction of the current flowing through windings $a1$ and $a2$, the rotor is displaced in any direction of the xoy plane, and finally the rotor is stably suspended. Assuming that the direction

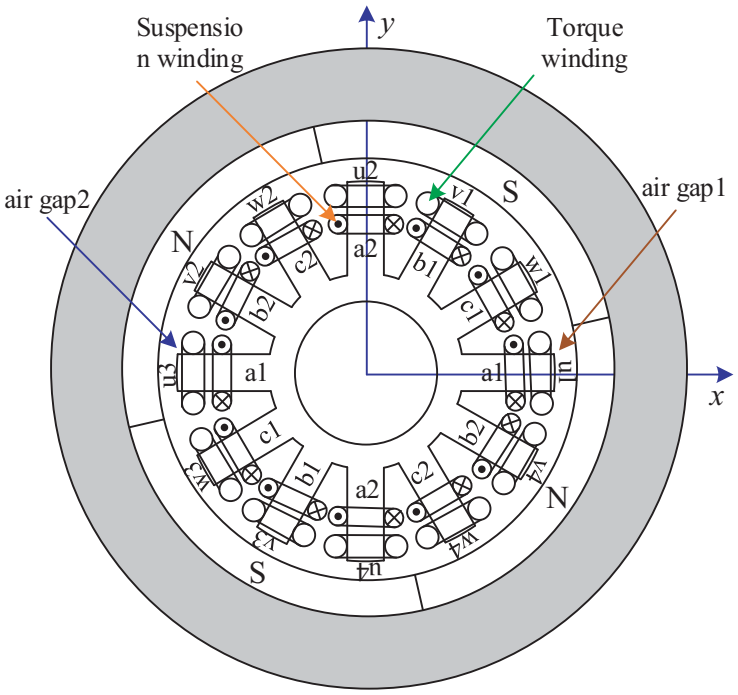

Figure 1. BBLDCM with Outer Rotor.

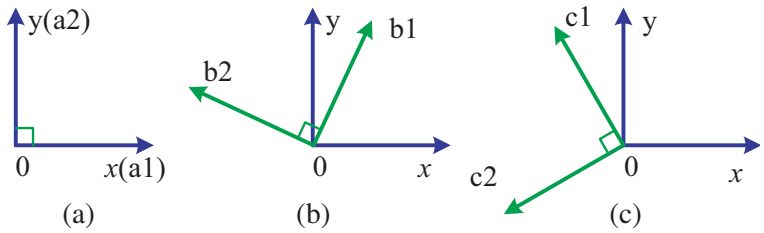

Figure 2. Coordinate of the levitation force of each phase. (a) Axis a1-a2. (b) Axis b1-b2. (c) Axis c1-c2.

of the suspension force generated by the suspension force winding is along axes $a1$, $a2$, $b1$, $b2$, $c1$, and $c2$, respectively, the coordinate systems $a1$-$a2$, $b1$-$b2$, and $c1$-$c2$ are established as shown in Fig. 2.

2.2. Model of Radial Suspension Force Model

The motor is placed vertically, so the radial suspension force does not take into account the effects of rotor gravity.

(1) When the motor rotor position angle $\theta < [0, 30°]$, the suspension force expression is:

$$\begin{bmatrix} F_x \\ F_y \end{bmatrix} = \begin{bmatrix} F_{sa1} \\ F_{sa2} \end{bmatrix} = k_i \begin{bmatrix} i_{a1} \\ i_{a2} \end{bmatrix} + k_x \begin{bmatrix} a_1 \\ a_2 \end{bmatrix} \tag{1}$$

where i_{a1} and i_{a2} are the currents flowing through the suspension windings $a1$ and $a2$; $a1$ and $a2$ are the displacements of the rotor $a1$-$a2$ in the coordinate system; k_i is the current stiffness coefficient, and k_x is the displacement stiffness coefficient.

(2) When the motor rotor position angle $\theta < [30°, 60°]$, the levitation force expression is:

$$\begin{bmatrix} F_x \\ F_y \end{bmatrix} = \begin{bmatrix} k_i i_{b1} + k_x b_1 \\ k_i i_{b2} + k_x b_2 \end{bmatrix} \begin{bmatrix} \cos 60° & \cos 150° \\ \sin 60° & \sin 150° \end{bmatrix} \tag{2}$$

(3) When the motor rotor position angle $\theta < [60°, 90°]$, the levitation force expression is:

$$\begin{bmatrix} F_x \\ F_y \end{bmatrix} = \begin{bmatrix} k_i i_{c1} + k_x c_1 \\ k_i i_{c2} + k_x c_2 \end{bmatrix} \begin{bmatrix} \cos 120° & \cos 240° \\ \sin 120° & \sin 240° \end{bmatrix} \tag{3}$$

2.3. Control of Suspension Force Control

For the closed-loop control of suspension force, it is necessary to observe the suspension force first. The estimation of suspension force can be calculated by Equations (1)–(3). At the same time, a two-point suspension force regulator is used, as shown in Fig. 3, to achieve high dynamic performance of motor rotor suspension control.

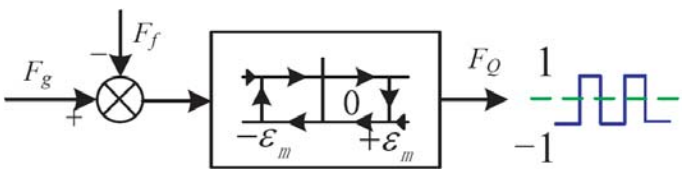

Figure 3. Two-point suspension force regulator.

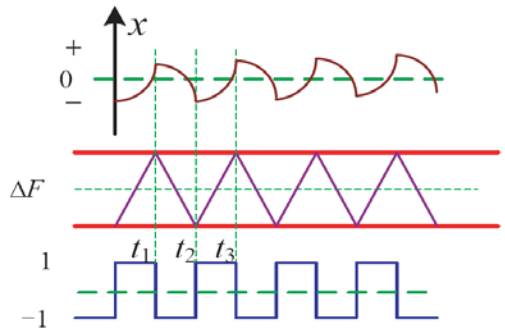

Figure 4. The working process of DSFC.

In Fig. 3, the input amount of the suspension force regulator is the error value ΔF of the suspension force set value F_g and the suspension force feedback value F_f, and the output amount F_Q is the switching signal of the suspension winding. The set tolerance of the suspension force regulator is $\pm\varepsilon m$, taking a discrete two-point adjustment. The specific adjustment process of the suspension force is shown in Fig. 4.

Taking the single-degree-of-freedom x-axis displacement direction as an example, when the rotor is eccentric $+x$ $(-x)$, the error value of the suspension force is less than (greater than) the lower tolerance limit set by the regulator $-\varepsilon m$ (upper tolerance limit $+\varepsilon m$). Then the output F_Q of the two-point regulator is changed to "-1" ("$+1$"). Under the control of $F_Q = -1$ ($F_Q = +1$), the motor suspension control subsystem conducts the corresponding suspension windings in reverse (forward) direction (the phase suspension winding is determined by the motor rotor position signal), which increases the radial suspension force along the $-x$ $(+x)$ direction and adjusts the rotor displacement to the center. It can be seen that the fluctuation of radial suspension force can be restrained within the allowable tolerance range by reasonably choosing the tolerance limit of the regulator $\pm\varepsilon m$, and the purpose of stable suspension of the motor rotor can be achieved finally.

2.4. Switch Table for Direct Suspension Force Winding Control

The winding of the BBLDCM is only a two-phase conduction in normal operation. Define a six-digit binary number to indicate the switching state of the inverter. Use "1" for on state and "0" for off state. The torque winding has six switch states: VT1 (010010), VT2 (000110), VT3 (100100), VT4 (100001), VT5 (001001), VT6 (011000); the floating winding has three switching states: VF1 (100100), VF2 (010010), VF3 (001001).

The motor selects and turns on the corresponding torque winding and suspension winding according to different logical combinations of three output signals HA, HB, and HC of the Hall position sensor to achieve continuous stable suspension operation. Taking Table 1 as an example, the corresponding relationships between the Hall signal and the torque winding and between the Hall signal and the conduction state of the suspension winding during motor operation is given.

Taking suspension winding $a1$ and $a2$ as examples, the switching table of direct suspension force winding is deduced. The non-zero suspension force vectors F_{sa1}, F_{sa2}, $-F_{sa1}$, and $-F_{sa2}$ can be generated in Fig. 5 when $a1$ and $a2$ suspension windings are working. The non-zero suspension force vectors divide the plane into four sectors. At the same time, the non-zero suspension force vectors can synthesize radial forces F_{a1}, F_{a2}, F_{a3}, and F_{a4} of different sizes and directions. When the eddy current displacement sensor detects that the rotor displacement (x, y) is in sector III, the radial force F_{a1} is selected to adjust the rotor displacement. In the same way, the conduction mode in other states can be obtained, and the direct suspension force winding switch table can be obtained as in Table 2.

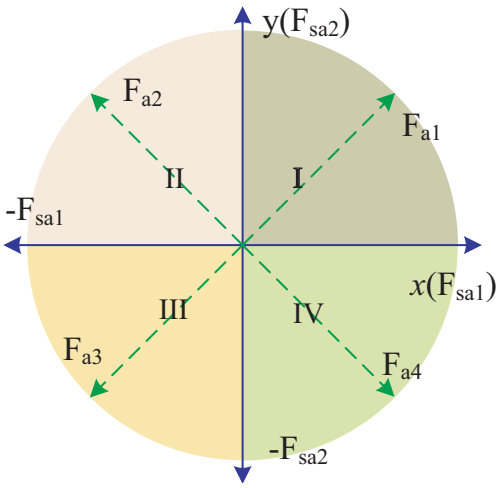

Figure 5. Suspension force vector generated by suspension winding.

Table 1. Motor clockwise rotation winding conduction table.

HA	HB	HC	Torque winding state	Suspension winding state
1	0	1	V_{T1} (010010)	V_{F2} (010010)
1	0	0	V_{T2} (000110)	V_{F1} (100100)
1	1	0	V_{T3} (100100)	V_{F3} (001001)
0	1	0	V_{T4} (100001)	V_{F2} (010010)
0	1	1	V_{T5} (001001)	V_{F1}(100100)
0	0	1	V_{T6} (011000)	V_{F3} (001001)

Table 2. Selection switch table for direct suspension force winding.

Sector	a-connected	b-connected	c-connected
I	F_{a3}	F_{b3}	F_{c3}
II	F_{a4}	F_{b4}	F_{c4}
III	F_{a1}	F_{b1}	F_{c1}
IV	F_{a2}	F_{b2}	F_{c2}

3. DESIGN OF SECOND-ORDER SLIDING MODE CONTROLLER

Suspension subsystem is a complex sensitive system, which is greatly affected by the outside world. In order to ensure the stability and dynamic performance of the control system, SOSM control is introduced into the BBLDCM suspension control subsystem.

3.1. Design of Second-Order Sliding Mode Displacement Controller

The suspension subsystem of BBLDCM is time-varying, non-linear, and has the characteristics of a variable structure. The control of rotor displacement is mainly changed in different control structures to meet the control requirements of stable suspension force. The structure of the SOSM-DSFC control is shown in Fig. 6.

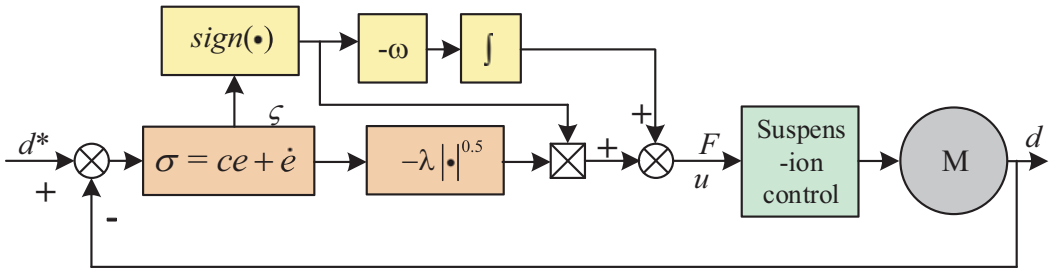

Figure 6. Schematic diagram of SOSM-DSFC.

The sliding mode displacement controller is designed by taking the x-axis single-degree-of-freedom displacement of the rotor as an example. Let the rotor x axial single degree of freedom displacement be d and the positioning displacement to d^*, the displacement tracking error can be expressed as:

$$e = d^* - d \tag{4}$$

Using a linear combination of e, $\dot{e}$, define the sliding mode variable as:

$$\sigma = ce + \dot{e} \tag{5}$$

where c is the gain factor, if the system moves to the sliding surface ($\sigma = 0$), then:

$$e(t) = e(t_0)e^{-c(t-t_0)} \tag{6}$$

In the formula, the value of the gain coefficient c determines the speed at which the sliding mode variable tends to zero.

Combining with the mathematical model of BBLDCM rotor suspension subsystem and Newton's law of motion, it can be concluded that:

$$m\ddot{d} = F_x + f_l \tag{7}$$

where F_x is the radial levitation force in the x-axis direction of the rotor; $F_x = k_x x + k_l i$, f_l is the radial interference force in the x-axis direction of the rotor; and m is the rotor mass of the motor. Since the suspension subsystem uses a DSFC structure, the radial levitation force in the x-axis direction of the rotor is defined as the control amount, that is, $u = F_x$

Let $y_1(t) = \sigma(t)$, $y_2(t) = \dot{\sigma}(t)$, and get:

$$\begin{cases} \dot{y}_1(t) = y_2(t) \\ \dot{y}_2(t) = c\ddot{d}^* + d^* + \dfrac{c}{\mathrm{m}}(f_l - u) - \dfrac{1}{\mathrm{m}}\dot{u} \end{cases} \tag{8}$$

In summary, the suspension force control problem of the BBLDCM suspension subsystem can be equivalent to the stability of the system within a certain period of time on the basis of the basic principle of the SOSM.

For the SOSM control law, the super twisting control algorithm is chosen. The algorithm does not need to calculate the derivative of the sliding mode variable and its symbol information, and $\sigma - \dot{\sigma}$ plane converges to the origin in a finite time. The second-order super-twisting control law is:

$$u\,(t) = u_1\,(t) + u_2\,(t) \tag{9}$$

and there are:

$$\begin{cases} \dot{u}_1 = \begin{cases} -u & |u| > 1 \\ -\omega \mathrm{sign}(\sigma), & |u| \le 1 \end{cases} \\ u_2 = \begin{cases} -\lambda\,|\sigma_0|^{\rho}\,\mathrm{sign}(\sigma), & |\sigma| > \sigma_0 \\ -\lambda\,|\sigma|^{\rho}\,\mathrm{sign}(\sigma), & |\sigma| \le \sigma_0 \end{cases} \end{cases} \tag{10}$$

where, ω, λ, ρ are the parameters to be set.

Due to the numerous parameters of the super-helical algorithm, the disturbance boundary is unknown, and the parameter debugging is difficult in practical engineering applications. Therefore, the generally simplified controller is selected as follows:

$$\begin{cases} u(t) = -\lambda_1\,|\sigma|^{0.5}\,\mathrm{sign}(\sigma) + Z \\ \dot{Z} = -\lambda_2 \mathrm{sign}(\sigma) \end{cases} \tag{11}$$

where $\sigma = ce + \dot{e}$, the control law has a simple structure, and the parameters are easy to adjust. The tuning method is similar to the Ziegler-Nichols tuning method in PID. First, λ_2 is set, and the value of λ_2 is increased until the output signal oscillates. Then the value of λ_2 is decreased until it is stable. The value of λ_2 is $85\% \sim 90\%$ at the time of oscillation. The tuning process of λ_1 is similar to λ_2 tuning process.

3.2. Improvement of Second-Order Sliding Mode Displacement Controller

In view of the requirements of the control precision, buffeting and robustness of the BBLDCM suspension subsystem, the linear control theory is combined with the optimization of the proposed SOSM displacement controller.

Consider the higher order derivative of the position error:

$$\begin{cases} F_x = \lambda_1\,|\sigma|^{1/2}\,\mathrm{sgn}(\sigma) + \lambda_2\sigma - Z \\ \dot{Z} = -\lambda_3 \mathrm{sgn}(\sigma) - \lambda_4\sigma \end{cases} \tag{12}$$

Uncertain bounded interference can be expressed as F_{R}=$F_{\mathrm{R0}} + k_{\mathrm{R}} f(t)$, which can be transformed into:

$$\xi_{\mathrm{R}}=\varepsilon_1 + \int_0^{\mathrm{t}} \varepsilon_2 dt \tag{13}$$

where ε_1, ε_2 is a boundary condition and can be written as:

$$\begin{cases} |\varepsilon_1|_{\max} = \left|\dfrac{\max(F_{\mathrm{R0}})}{m}\right| + |cv|_{\max} + \left|c\dot{d}^*\right|_{\max} \\ |\varepsilon_2|_{\max} = \max(\mathrm{k_R k_T}) \end{cases} \tag{14}$$

where v is the displacement velocity of the suspended rotor. Rewrite Equation (12) into a vector form, with $z = [z_1, z_2]^{\mathrm{T}}$, where z_1=σ, z_2=Z+$\int_0^t \varepsilon_2(\tau)\mathrm{d}\tau$. Then the bounded condition of ε_1, ε_2 can be written as:

$$\begin{cases} |\varepsilon_1| \le \left[\Delta_1 |z_1|^{1/2} + \Delta_3 |z_1|\right] \\ |\varepsilon_2| \le \Delta_3 + \Delta_4 |z_1| \end{cases} \tag{15}$$

where $\Delta_1 > 0$, $\Delta_2 > 0$, $\Delta_3 > 0$, $\Delta_4 > 0$. The closed-loop system equation can be obtained by derivation and arrangement of Z:

$$\begin{cases} \dot{z}_1 = \left[\lambda_1 |z_1|^{1/2} \operatorname{sgn}(\sigma) + \lambda_2 z_1 - z_2 + \varepsilon_1\right] \\ \dot{z}_2 = -\lambda_3 \operatorname{sgn}(\sigma) - \lambda_3 z_1 + \varepsilon_2 \end{cases} \tag{16}$$

3.3. Stability Analysis

Construct the Lyapunov function and simplify it to a quadratic form:

$$\begin{aligned} V &= 2\lambda_3 |z_1| + \lambda_4 z_1^2 + 0.5 z_2^2 + 0.5 \left(\lambda_1 |z_1|^{0.5} \operatorname{sgn}(z_1) + \lambda_2 z_1 - z_2\right)^2 \\ &= \zeta^{\mathrm{T}} \Pi \zeta \end{aligned} \tag{17}$$

where $\zeta^{\mathrm{T}} = [|z_1|^{0.5}\operatorname{sgn}(z_1), z_1, z_1]$, $\|\zeta\|^2 = |z_1| + z_1^2 + z_2^2$, $\|\zeta\|^2$ is the norm of ζ and

$$\Pi = 0.5 \begin{bmatrix} 4\lambda_3 + \lambda_1^2 & \lambda_1\lambda_2 & -\lambda_1 \\ \lambda_1\lambda_2 & 2\lambda_4 + \lambda_2^2 & -\lambda_2 \\ -\lambda_1 & -\lambda_2 & 2 \end{bmatrix}.$$

When $\lambda_1 > 0$, $\lambda_2 > 0$, $\lambda_3 > 0$, $\lambda_4 > 0$, Π is a positive definite matrix. If $\mathrm{z}_1 \neq 0$, then V can be continuously different and has the following relationship:

$$L_{\min}(\Pi) \|\zeta\|^2 \le V \le L_{\max}(\Pi) \|\zeta\|^2 \tag{18}$$

where $L_{\min}(\Pi)$ represents the minimum eigenvalue of Π; $L_{\max}(\Pi)$ represents the largest eigenvalue of Π.

$$\dot{V} = \frac{1}{|z_1|^{0.5}} \zeta^{\mathrm{T}} \Theta_1 \zeta - \zeta^{\mathrm{T}} \Theta_2 \zeta + \varpi_1^{\mathrm{T}} \zeta + \frac{1}{|z_1|^{0.5}} \varpi_2^{\mathrm{T}} \zeta \tag{19}$$

where,

$$\Theta_1 = \frac{1}{2}\lambda_1 \begin{bmatrix} 2\lambda_3 + \lambda_1^2 & 0 & -\lambda_1 \\ 0 & 2\lambda_4 + 5\lambda_2^2 & -3\lambda_2 \\ -\lambda_1 & -3\lambda_2 & 1 \end{bmatrix}, \quad \Theta_2 = \lambda_2 \begin{bmatrix} \lambda_3 + 2\lambda_1^2 & 0 & 0 \\ 0 & \lambda_4 + \lambda_2^2 & -\lambda_2 \\ 0 & -\lambda_2 & 1 \end{bmatrix},$$

$$\varpi_1^{\mathrm{T}} = \begin{bmatrix} \lambda_1(1.5\lambda_2\delta_1 - \delta_2) & \left(\lambda_2^2 + 2\lambda_4\right)\delta_1 + \lambda_2\delta_2 & -\lambda_2\delta_1 \end{bmatrix}, \quad \varpi_2^{\mathrm{T}} = \delta_1 \begin{bmatrix} 2\lambda_3 + 0.5\lambda_1^2 & 0 & 0.5\lambda_1 \end{bmatrix}.$$

From the boundary formula of the interference function:

$$\begin{cases} \dfrac{1}{|z_1|^{0.5}} \varpi_2^{\mathrm{T}} \zeta \le \dfrac{\Delta_1}{|z_1|^{0.5}} \zeta^{\mathrm{T}} \Omega_1 \zeta + \Delta_3 \zeta^{\mathrm{T}} \Omega_1 \zeta \\ \varpi^{\mathrm{T}} \le \dfrac{1}{|z_1|^{0.5}} \zeta^{\mathrm{T}} \Omega_2 \zeta + \zeta^{\mathrm{T}} \Omega_3 \zeta \end{cases} \tag{20}$$

where,

$$\Omega_1 = \begin{bmatrix} 2\lambda_3 + 0.5\lambda_1^2 & 0 & 0.25\lambda_1 \\ 0 & 0 & 0 \\ 0.25\lambda_1 & 0 & 0 \end{bmatrix}, \quad \Omega_2 = \begin{bmatrix} \Delta_2\lambda_1 & 0 & 0 \\ 0 & \lambda_1\left(1.5\lambda_2\Delta_3 + \Delta_4\right) + \left(\lambda_2^2 + 2\lambda_4\right)\Delta_1 & 0 \\ 0 & 0 & 0 \end{bmatrix}$$

and

$$\Omega_3 = \begin{bmatrix} \lambda_2\left(\Delta_2 + 1.5\lambda_1\Delta_1\right) & 0 & 0.5\lambda_2\Delta_1 \\ 0 & \left(\lambda_2^2 + 2\lambda_4\right)\Delta_3 + \lambda_2\Delta_4 & 0.5\lambda_2\Delta_3 \\ 0.5\lambda_2\Delta_1 & 0.5\lambda_2\Delta_3 & 0 \end{bmatrix}.$$

The first derivative of Lyapunov function can be written as follows:

$$\dot{V} = -\frac{1}{|z_1|^{1/2}}\zeta^{\mathrm{T}}\left(\Theta_1 - \Omega_2 - \Delta_1\Omega_1\right)\zeta - \zeta^{\mathrm{T}}\left(\Theta_2 - \Omega_3 - \Delta_3\Omega_1\right)\zeta \tag{21}$$

Lyapunov stability criterion $\dot{V} < 0$, that is, the condition that σ, $\dot{\sigma}$ tends to zero in a certain period of time is equivalent to the discrimination of the positive definite matrix $(\Theta_1 - \Omega_2 - \Delta_1\Omega_1)$, $(\Theta_2 - \Omega_3 - \Delta_3\Omega_1)$. When λ_1, λ_2, λ_3, λ_4 satisfies Eq. (22), $(\Theta_1 - \Omega_2 - \Delta_1\Omega_1 = 0)$.

$$\begin{cases} \lambda_1 > 2\max\left(\Delta_1, \sqrt{\Delta_2}\right) \\ \lambda_2 > \dfrac{3}{8}\Delta_3 + \dfrac{1}{4}\sqrt{\dfrac{9}{4}\Delta_3^2 + 8\Delta_4} \\ \lambda_3 > \lambda_1\dfrac{\Delta_1\lambda_1 + \dfrac{1}{8}\lambda_1^2 + \lambda_2}{2\left(\dfrac{1}{2}\lambda_1 - \lambda_1\right)} \\ \lambda_4 > \dfrac{\lambda_1\left[\dfrac{1}{2}\lambda_1\left(\lambda_1 + \dfrac{1}{2}\Delta\right)^2\left(2\lambda_2^2 - \dfrac{3}{2}\Delta_3\lambda_2 - \Delta_4\right) + \left(\dfrac{5}{2}\lambda_2^2 + \dfrac{3}{2}\lambda_2\Delta_3 + \Delta_4\right)\right]p_1}{2\left(p_1 - \dfrac{1}{2}\lambda_1\left(\lambda_1 + \dfrac{1}{2}\Delta_1\right)^2\right)\left(\dfrac{1}{2}\lambda_1 - \Delta_1\right)} - \dfrac{1}{2}\lambda_2 \end{cases} \tag{22}$$

where $p_1 = \lambda_1\left(\frac{1}{4}\lambda_1^2 - \Delta_2\right) + (\frac{1}{2}\lambda_1 - \Delta_1)(2\lambda_3 + \frac{1}{2}\lambda_1^2)$.

Simplify $\zeta^{\mathrm{T}}(\Theta_2 - \Omega_3 - \Delta_3\Omega_1)\zeta$ to get:

$$\zeta^{\mathrm{T}}\left(\Theta_2 - \Omega_3 - \Delta_3\Omega_1\right)\zeta = \eta^{\mathrm{T}}\vartheta_1\eta + z^{\mathrm{T}}\vartheta_2 z \tag{23}$$

where,

$$\vartheta_1 = \begin{bmatrix} \lambda_2\left(\left(\lambda_3 + 2\lambda_1^2\right) - \Delta_2 - \dfrac{3}{2}\lambda_1\Delta_1\right) - \left(2\lambda_3 + \dfrac{\lambda_1^2}{2}\right)\Delta_3 & -\dfrac{1}{2}\left(\lambda_2\Delta_3 + \dfrac{\lambda_1^2}{2}\right)\Delta_3 \\ -\dfrac{1}{2}\left(\lambda_2\Delta_1 + \dfrac{1}{2}\lambda_1\Delta_3\right) & \dfrac{1}{2}\lambda_2 \end{bmatrix},$$

$$\vartheta_2 = \begin{bmatrix} \lambda_2\left(\lambda_4 + \lambda_2^2\right) - \left(\lambda_2^2 + 2\lambda_4\right)\Delta_3 - \lambda_2\Delta_4 & -\lambda_2\left(\lambda_2 + \dfrac{1}{2}\Delta_3\right) \\ -\lambda_2\left(\lambda_2 + \dfrac{1}{2}\Delta_3\right) & \dfrac{1}{2}\lambda_2 \end{bmatrix}.$$

To verify whether matrix $\zeta^{\mathrm{T}}(\Theta_2 - \Omega_3 - \Delta_3\Omega_1)\zeta$ is positive definite, the inequality conditions to be

satisfied are as follows:

$$\begin{cases} \lambda_2 > 2\Delta_3 \\ \lambda_3 > \dfrac{\left(\lambda_2\Delta_1 + \dfrac{1}{2}\lambda_1\Delta_3\right)^2}{2\lambda_2(\lambda_2 - 2\Delta_3)} + \dfrac{\left(\Delta_2 + \frac{3}{2}\Delta_1\lambda_1\right)\lambda_2 - 2\left(\lambda_2 - \dfrac{1}{4}\Delta_3\right)\lambda_1^2}{\lambda_2 - 2\Delta_3} \\ \lambda_3 > \dfrac{\left(\lambda_2\Delta_1 + \dfrac{1}{2}\lambda_1\Delta_3\right)^2}{2\lambda_2\left(\lambda_2 - 2\Delta_3\right)} + \dfrac{\left(\Delta_2 + \frac{3}{2}\Delta_1\lambda\right)}{2} + \dfrac{\lambda_2 - 2\left(\lambda_2 - \frac{1}{4}\Delta_3\right)/4^2}{\lambda_2 - 2\Delta_3} \\ \lambda_4 > \lambda_2\dfrac{\left[\lambda\left(\lambda_2 + 3\Delta_3\right) + \dfrac{1}{2}\Delta_3^2 + \Delta_4\right]}{\lambda_2 - 2\Delta_3} \end{cases} \tag{24}$$

In summary, when Equations (23) and (24) are established, $(\Theta_1 - \Omega_2 - \Delta_1\Omega_1)$, $(\Theta_2 - \Omega_3 - \Delta_3\Omega_1)$ is a positive definite matrix; the stability condition $\dot{V} < 0$ is established; and the system in Eq. (16) converges in a finite time. From Eq. (17):

$$\begin{cases} \|\zeta\|_{\max} = V^{1/2}/L_{\min}^{1/2}(\Pi) \geq \|\zeta\| \geq V^{1/2}/L_{\max}^{1/2}(\Pi) = \|\zeta\|_{\min} \\ \|\zeta\| \geq |z_1|^{1/2} \\ \|\zeta\| \geq \|\zeta\|_{\min}^2 / \|\zeta\|_{\max} \\ \|\zeta\|^2 \geq |z_1|^{1/2} L_{\min}^{1/2}(\Pi) / L_{\max}(\Pi) V^{1/2} \\ \|\zeta\|^2 \geq 1/L_{\max}(\Pi) V \end{cases} \tag{25}$$

Therefore,

$$\begin{cases} \zeta^{\mathrm{T}}\left(\Theta_1 - \Omega_2 - \Delta_1\Omega_1\right)\zeta \geq \lambda_{\min}\left(\Theta_1 - \Omega_2 - \Delta_1\Omega_1\right)\|\zeta\|^2 \\ \zeta^{\mathrm{T}}\left(\Theta_2 - \Omega_3 - \Delta_3\Omega_1\right)\zeta \geq \lambda_{\min}\left(\Theta_2 - \Omega_3 - \Delta_3\Omega_1\right)\|\zeta\|^2 \end{cases} \tag{26}$$

Find the first derivative of the Lyapunov function with respect to time:

$$\dot{V} \leq -\gamma_1 V^{1/2} - \gamma_2 V \tag{27}$$

where,

$$\begin{cases} \gamma_1 = \lambda_{\min}\left(\Theta_1 - \Omega_2 - \Delta_1\Omega_1\right)\lambda_{\min}^{1/2}(\Pi)/\lambda_{\max}(\Pi) \\ \gamma_2 = \lambda_{\min}\left(\Theta_2 - \Omega_3 - \Delta_3\Omega_1\right)/\lambda_{\max}(\Pi) \end{cases} \tag{28}$$

Solve the following differential equations,

$$\begin{cases} \dot{V} = -\gamma_1 V^{1/2} - \gamma_1 V \\ V(0) = V_0 \\ V(T_{\mathrm{c}}) = 0 \end{cases} \tag{29}$$

Thus, $T_{\mathrm{c}} = \frac{2}{\gamma_2}\ln(1 + \gamma_2/\gamma_1 V_0^{1/2})$, and Eq. (16) can approach the equilibrium point at T_{c} certain time.

4. SIMULATION AND RESULT ANALYSIS

The direct suspension force control strategy based on SOSM control and the DSFC strategy based on PID control are based on MATLAB/Simulink simulation platform to build a simulation model, perform simulation comparisons by keeping the set parameters unchanged and setting radial interference and radial interference-free, respectively, and then carry out related research.

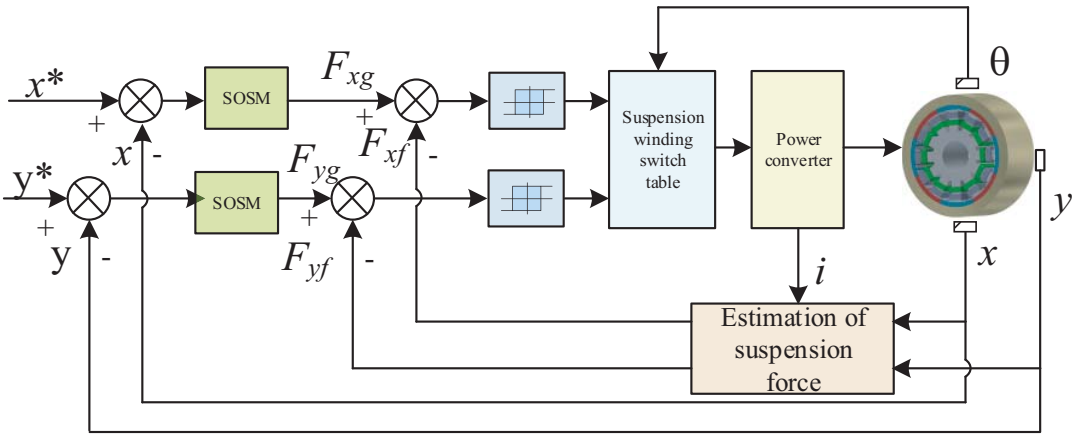

Figure 7. Diagram of DSFC for suspension subsystem of BBLDCM.

4.1. Structure Block Diagram of Suspension Control Subsystem

The block diagram of the DSFC of the suspension system of the magnetic suspension brushless DC motor is shown in Fig. 7. In the figure, $x*$ and $y*$ are the given rotor displacements, respectively, and x and y are the motor rotors x and y actually detected by the eddy current sensor. F_{xg}, F_{yg} are the given levitation force, and F_{xf}, F_{yf} are the actual radial suspension force of the rotor. The displacement errors $x^* - x$ and $y^* - y$ are generated by the SOSM controller. The suspension force errors are output by the suspension force two-point regulator to the switching signal of the suspension winding. The conducting phase of the suspension winding is selected according to the rotor position signal. Finally, the suspension subsystem of the motor is controlled by the power converter.

4.2. Analysis of Simulation Results without Radial Interference

Figure 8 shows a simulation result of rotor displacement control by direct suspension force control with improved SOSM. After adding the improved SOSM, the time for the motor rotor to return to the center position is 0.25 s, and it can be seen that the rotor does not show overshoot during the dynamic displacement. After the rotor moves to the center position, it is shaken between -0.02 mm ~ 0.012 mm from the center position, and the maximum jitter amplitude is 0.032 mm.

Figure 9 shows the results of simulation of rotor displacement based on PID direct suspension force control. When the rotor is operated under the direct suspension force control based on PID, the maximum displacement amplitude of the x-axis in the initial rotor is -0.06 mm, and the maximum displacement amplitude in the y-axis is 0.05 mm. After 0.3 s, the rotor is stably suspended between -0.025 mm and 0.03 mm, and the maximum jitter amplitude is 0.055 mm.

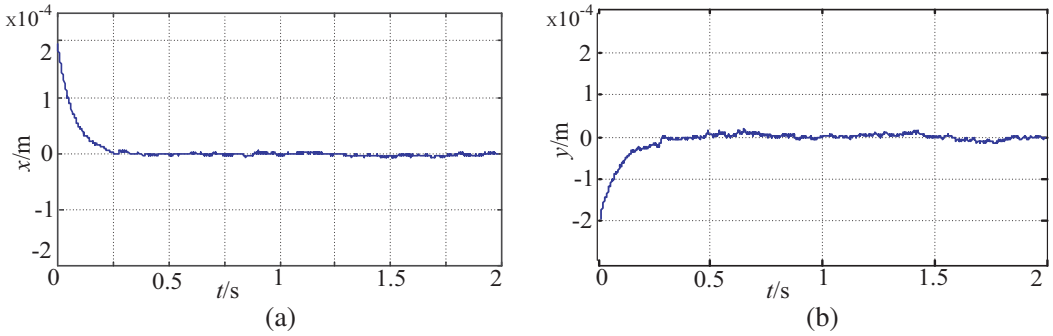

Figure 8. Rotor position with SOSM-DSFC method. (a) x-axis rotor displacement. (b) y-axis rotor displacement.

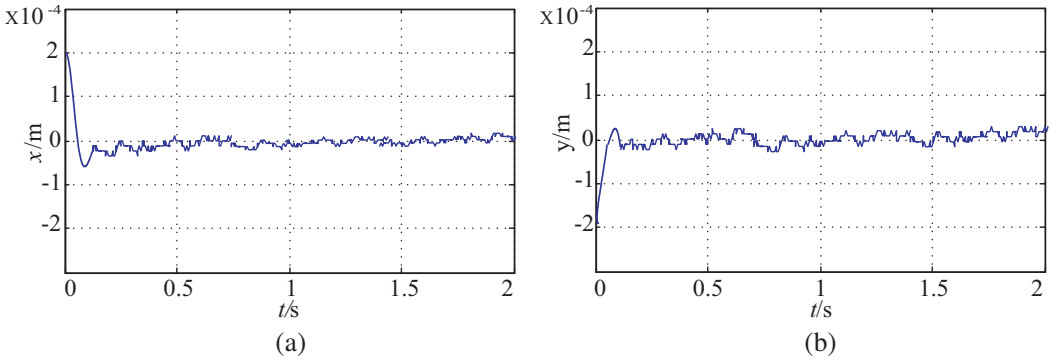

Figure 9. Rotor position with PID-DSFC method. (a) x-axis rotor displacement. (b) y-axis rotor displacement.

In general, compared with the direct suspension force control strategy based on PID control, the rotor damping suppression performance is improved by 51% based on the improved second-order sliding mode direct suspension force control, and the dynamic response performance of the suspension rotor is also greatly improved.

4.3. Analysis of Simulation Results under Radial Interference

In order to verify the robust performance of the proposed control scheme, radial disturbance force is applied to the suspension control subsystem to observe the displacement trajectory of the rotor under external disturbance.

Figure 10 shows the radial suspension force and displacement trajectory of the rotor under the control of direct suspension force based on PID. Fig. 10(a) shows x-axis rotor displacement trajectory. After the suspension rotor is stably operated, the radial interference force in the x-axis is applied at 1 s.

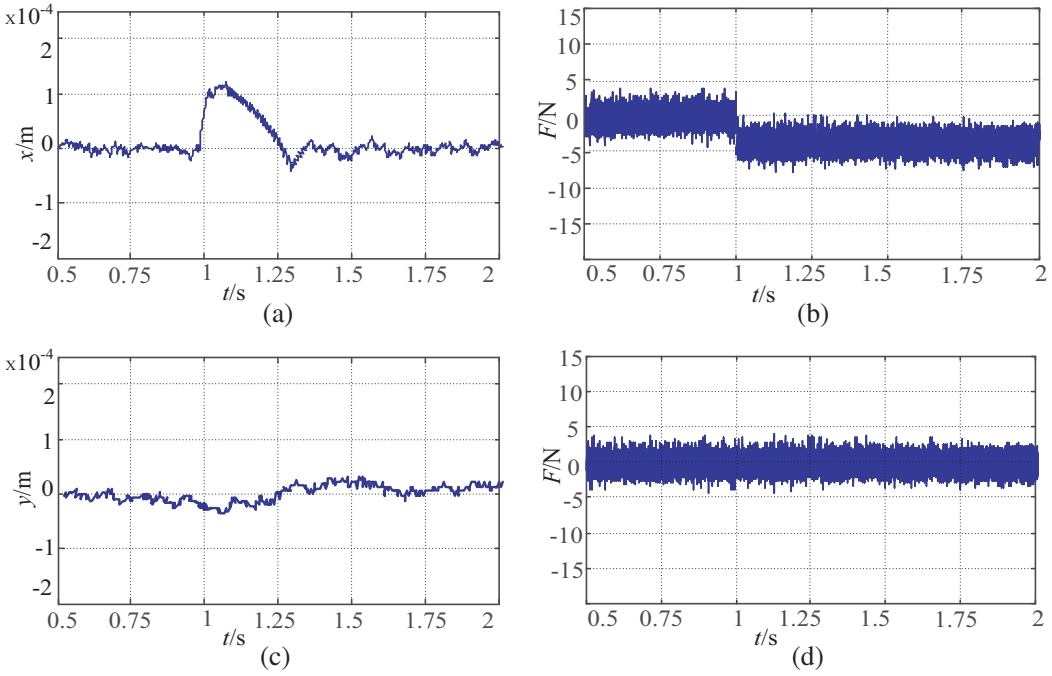

Figure 10. Rotor position and suspension with PID-DSFC method. (a) x-axis rotor displacement. (b) x-axis suspension force. (c) y-axis rotor displacement. (d) y-axis suspension force.

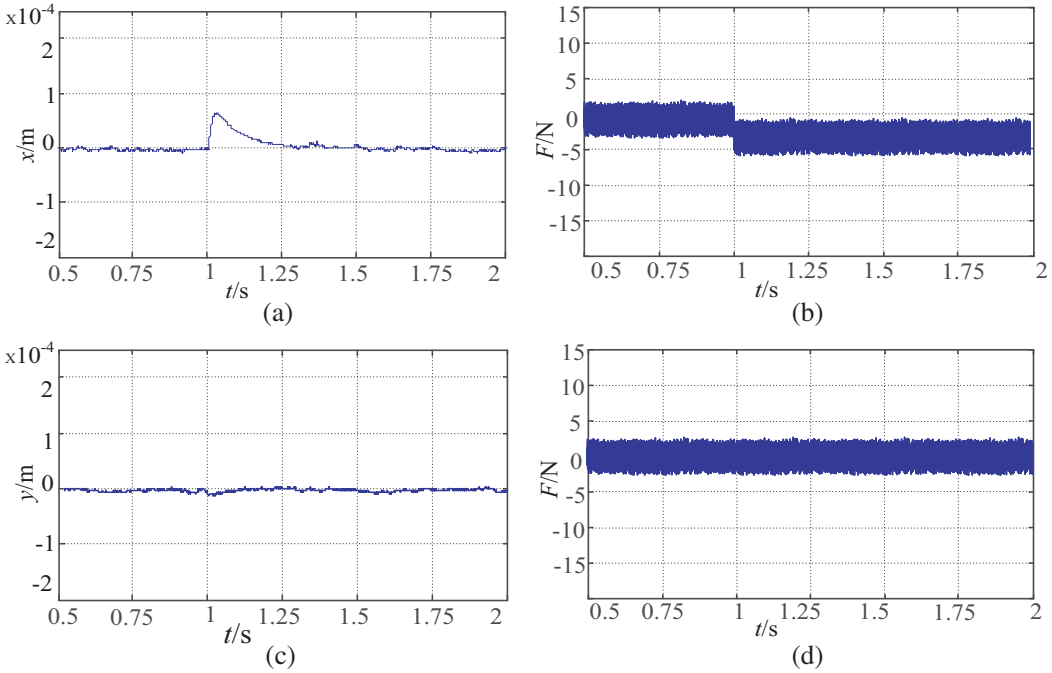

Figure 11. Rotor position and suspension with SOSM-DSFC method. (a) x-axis rotor displacement. (b) x-axis suspension force. (c) y-axis rotor displacement. (d) y-axis suspension force.

Under the action of radial force, the rotor controlled by direct suspension force is eccentric to 0.12 mm from the center position and restores stability within 0.3 s, with a small overshoot. Fig. 10(b) is the corresponding suspension force waveform after radial interference. After receiving the interference force, the corresponding suspension force value increases. Fig. 10(c) and Fig. 10(d) show the y-axis suspension force and displacement after the rotor is disturbed in the x-axis. After the x-axis is disturbed, the rotor y-axis is slightly affected.

Figure 11 shows the displacement trajectory and suspension force waveform of the rotor based on the second-order sliding mode direct levitation force control under radial disturbance. Fig. 11(a) shows the x-axis rotor displacement trajectory. Under the action of the x-axis interference force, when the rotor is operating stably, the system axis is used as the reference offset to not exceed 0.07 mm, which is 42% lower than the displacement deviation based on the PID direct suspension force control strategy, indicating that the rotor vibration problem has been improved. It returns to the center position at 0.25, stabilizes the suspension, no overshoot, and has a 33% increase in dynamic response speed compared to the PID method. Fig. 11(b) shows the suspension force in the x-axis of the rotor. Under the influence of interference, the corresponding suspension force increases.

A comprehensive analysis of Figs. 8–11 shows that the SOSM controller based on the DSFC strategy further enhances the robustness of the suspension subsystem, effectively reduces the external suspension to the stable suspension of the rotor, and improves the control accuracy of the suspension subsystem.

5. CONCLUSION

Aiming at the shortcomings of DSFC method for BBLDCM, a new type of DSFC strategy based on improved SOSM control is proposed. The mathematical model of SOSM controller is deduced, and the new model is clarified. The working principle and adjusting process of the new direct suspension force are expounded. Results show that the improved second-order sliding mode controller is based on the PID direct suspension force control strategy, which further enhances the robustness of the suspension subsystem, effectively reduces the influence of external disturbance on the stable suspension of the rotor, and improves the control accuracy of suspension subsystem.

ACKNOWLEDGMENT

This work was sponsored by the National Natural Science Foundation of China (51707082); Humanities and Social Sciences Research Project of Henan Education Department (2019-ZDJH-135).

REFERENCES

1. Yuan, Y., Y. Sun, and Y. Huang, "Design and analysis of bearingless flywheel motor specially for flywheel energy storage," *IET Electronics Letters*, Vol. 52, No. 16, 66–68, Jan. 2016.
2. Ooshima, M. and C. Takeuchi, "Magnetic suspension performance of a bearingless brushless DC motor for small liquid pumps," *IEEE Transactions on Industry Applications*, Vol. 47, No. 1, 72–78, Jan.–Feb. 2011.
3. Murashige, T. and W. Hijikata, "Mechanical antithrombogenic properties by vibrational excitation of the impeller in a magnetically levitated centrifugal blood pump," *Artificial Organs*, Vol. 43, No. 9, 849–859, Sep. 2019.
4. Jing, L., J. Cheng, and T. Ben, "Analytical method for magnetic field and electromagnetic performances in switched reluctance machines," *Journal of Electrical Engineering & Technology*, Vol. 14, No. 4, 1625–1635, Jul. 2019.
5. Severson, E. L., "Bearingless motor technology for industrial and transportation applications," *IEEE Transportation and Electrification Conference and Expo*, 266–273, Long Beach, CA, USA, 2018.
6. Zwyssig, C., T. Baumgartner, and J. W. Kolar, "High-speed magnetically levitated reaction wheel demonstrator," *2014 International Power Electronics Conference*, IEEE, 2014.
7. Jing, L., J. Gong, Z. Huang, T. Ben, and Y. Huang, "A new structure for the magnetic gear," *IEEE Access*, Vol. 7, 75550–75555, 2019.
8. Zhu, X., J. Huang, L. Quan, Z. Xiang, and B. Shi, "Comprehensive sensitivity analysis and multi-objective optimization research of permanent magnet flux-intensifying motors," *IEEE Transactions on Industrial Electronics*, Vol. 66, No. 4, 2613–2627, Apr. 2019.
9. Zhu, X., Z. Shu, L. Quan, Z. Xiang, and X. Pan, "Design and multi-condition comparison of two outer-rotor flux-switching permanent magnet motors for in-wheel traction applications," *IEEE Transactions on Industrial Electronics*, Vol. 64, No. 8, 6137–6148, 2017.
10. Grabner, H., W. Amrhein, and S. Silber, "Nonlinear feedback control of a bearingless brushless DC motor," *IEEE-ASME Transactions on Mechatronics*, Vol. 15, No. 1, 40–47, Feb. 2010.
11. Yuan, Y., Y. Huang, and Y. Sun, "Mathematical modeling and control for a single winding bearingless flywheel motor in electric/suspension mode," *Journal of Electrical Engineering & Technology*, Vol. 13, No. 5, 1935–1944, Sep. 2018.
12. Zhu, H. and L. Shan, "A new control method of suspension force for bearingless brushless DC motor," *Journal of Jiangsu University (Natural Science Edition)*, Vol. 36, No. 2, 209–214, Feb. 2015.
13. Henzel, M., K. Falkowski, and M. Żokowski, "The analysis of the control system for the bearingless induction electric motor," *Journal of Vibroengineering*, Vol. 14, No. 1, 16–21, Mar. 2012.
14. Deng, Z., H. Zhang, and X. Wang, " The nonlinear decoupling control of the bearingless induction motors based on the airgap flux orientation," *Chinese Journal of Aeronautics*, Vol. 15, No. 1, 38–42, Feb. 2002.
15. Nian, H., Y. He, and L. Huang, "Integrated self-sensing of rotor position and displacement for inset PM type bearingless motor," *Proceedings of the CSEE*, Vol. 27, No. 9, 52–58, Mar. 2007.
16. Qiu, Z., Z. Deng, and Y. Zhang, "Direct levitation force control of a consequent-pole permanent magnet bearingless motor," *Transactions of China Electrotechnical Society*, Vol. 26, No. 9, 94–99, Sep. 2011.
17. Liu, H., J. Wang, and J. Zhang, "Research on torque ripple suppression techniques for brushless DC motor," *2013 the 25th Chinese Control and Decision Conference (CCDC)*, 424–429, 2013.

18. Ammar, A., A. Bourek, and A. Benakcha, "Nonlinear SVM-DTC for induction motor drive using input-output feedback linearization and high order sliding mode control," *ISA Transactions*, Vol. 67, 428–442, Mar. 2017.
19. Sun, Y., K. Zhang, and Y. Yuan, "A novel direct suspension force control for bearingless brushless DC motor," *Electric Machines & Control Application*, Vol. 45, No. 11, 1–6, 2018.
20. Masmoudi, M., B. El Badsi, and A. Masmoudi, "direct torque control of brushless DC motor drives with improved reliability," *IEEE Transactions on Industry Applications*, Vol. 50, No. 6, 3744–3753, Nov.–Dec. 2014.
21. Ozturk, S. B., W. C. Alexander, and H. A. Toliyat, "Direct torque control of four-switch brushless DC motor with non-sinusoidal back EMF," *IEEE Transactions on Power Electronics*, Vol. 25, No. 2, 263–271, Feb. 2010.